Appl Phys B (2009) 96: 821–826
DOI 10.1007/s00340-009-3688-4

Applied Physics B
Lasers and Optics

Second-harmonic generation spectroscopy on organic nanofibers

K. Pedersen · M. Schiek · J. Rafaelsen · H.-G. Rubahn

Received: 18 November 2008 / Revised version: 10 June 2009 / Published online: 8 August 2009

Abstract Optical second-harmonic generation upon nanosecond laser irradiation of nanofibers grown from nonsymmetrically functionalized *para*-quarter-phenylene molecules on mica surfaces is investigated in the spectral region around electronic resonances. Strong multiphoton excited luminescence appears together with the second-harmonic signal in the spectra. It is demonstrated how the two components can be separated by analyzing emission spectra recorded over a broad range of wavelengths around the second-harmonic energy. Spectra of the absolute values of the second-harmonic signals are obtained for three differently functionalized molecules. Together with supplementary measurements of the structure of the nanofiber films this forms the basis for estimation of the second-harmonic susceptibility of the fiber materials. Values of the nonlinear susceptibilities are obtained, which are comparable to those of well-known inorganic nonlinear optical crystals.

PACS 42.65.Ky · 78.55.Kz · 72.80.Le · 81.07.-b

1 Introduction

Organic nanofibers have potential applications as highly efficient nonlinear optical elements, such as electro-optical modulators and frequency converters, in modern integrated optics [1]. Second-order optical nonlinearities can be obtained by growing the wires from organic molecules with intrinsic hyperpolarizabilities. Semiconducting organics, such as *para*-phenylenes, can be functionalized with electron push and pull groups to introduce a permanent dipole moment in the molecules [2, 3]. Such molecules have been grown as oriented crystals forming parallel needle shaped nanofibers by a self-assembly process on muscovite mica substrates [4, 5]. The nanofibers may be used as grown on the mica substrate or they may be transferred to another substrate as building blocks in the process of forming nanoscale nonlinear optical structures.

Optical second-harmonic generation (SHG) spectroscopy is a useful tool for characterization of nonlinear optical structures for integrated optics as it has been demonstrated for inorganic systems, for instance poled glasses [6] and nanowires [7–13]. Furthermore, the spatial distribution of nonlinearities can be determined with SHG microscopy [14, 15]. Also organic structures can be investigated for second-order nonlinear effects with SHG. However, for organic systems frequency-doubled light often appears together with two-photon photoluminescence (PL), usually covering a broad spectral range due to coupling to a number of vibrational modes. In cases with strong two-photon PL isolation of the SHG part of the spectrum may require second-order spectroscopy over a broad wavelength range.

Previous works have presented experimental results for second-order susceptibilities of organic systems forming nanofibers obtained with light pulses in the femtosecond regime [16, 17]. In the present work the dispersion of the SH response of nanofibers formed by three different organic materials is analyzed and the absolute nonlinear susceptibilities are estimated on the basis of spectroscopy with nanosecond

K. Pedersen (✉) · J. Rafaelsen
Department of Physics and Nanotechnology, Aalborg University, Skjernvej 4A, 9220 Aalborg øst, Denmark
e-mail: kp@nano.aau.dk
Fax: +45-98156502

M. Schiek · H.-G. Rubahn
NanoSYD, Mads Clausen Institute, University of Southern Denmark, Alsion 2, 6400, Sønderborg, Denmark

(ns) pulses. The relatively low average power of ns parametric oscillators leads to stable signals without photobleaching and thus allows investigations of the same sample area over long time. Furthermore, the ease of wavelength scanning of ns parametric oscillators facilitates detailed spectroscopy over a broad range covering the lowest resonance frequency of the nonlinear response and thus separation of SHG from two-photon photoluminescence.

2 Experimental details

Ordered structures of nanofibers have been produced by deposition of the organic material on muscovite mica substrates. Details concerning the synthesis of the molecules can be found in Refs. [2, 3] and the nanofiber growth procedure on mica is described in Ref. [5]. Investigations of the bare mica substrates showed no detectable SHG signal. Three different molecules were investigated here all having four phenylene rings, but with different end groups: Methoxy-Cyano-*p*-Quaterphenylene (MOCNP4), Methoxy-Chloro-*p*-Quaterphenylene (MOCLP4), 1-Cyano-*p*-Quaterphenylene (CNHP4). The structures of the molecules are shown in Fig. 1.

The SHG spectroscopy experiments have been performed using a Nd:YAG-laser pumped optical parametric oscillator (OPO) system delivering 5-ns pulses at 10-Hz repetition rate. Average output powers of the OPO were typically around 10 mW. The light from the OPO was focused to a 1-mm spot on the sample at normal incidence and the spectral composition of the up-converted transmitted light was investigated with a monochromator. A photomultiplier tube coupled to gated electronics was used to detect the nonlinear signals. In order to normalize SH signals from the nanofiber samples reference spectra were recorded in reflection from a wedge-shaped (30°) quartz crystal placed at the position of the sample. This gives a reference signal without Maker fringes and with a magnitude comparable to that of the sample signals.

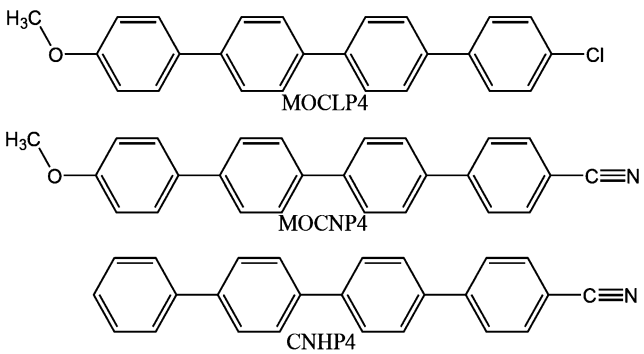

Fig. 1 Molecular forms of the three nonsymmetrically functionalized *para*-quaterphenylenes

3 Experimental results

The structure of the deposited nanofiber films has been analyzed with AFM in order to determine distributions of heights, widths, and fractional surface coverage of the wires. Figure 2 shows a scan of a MOCNP4 nanofiber film. It is seen that the fibers are well-aligned along a preferred direction. Interaction between the substrate and organic material favors growth along the [110] direction and molecules oriented almost perpendicular to the axis of the fibers. As described by Brewer et al. the SH signal is proportional to the square of the wire height for wires in the range of a few hundred nanometers as investigated here [16]. The important parameter for SHG is thus the average of the square of the wire height. Investigations of several AFM scans on the three nanofiber samples have led to the parameters shown in Table 1.

Figure 3 shows a spectrum from MOCLP4 wires excited by 720-nm pump light. A peak at the SH wavelength can clearly be identified, but a broad luminescence peak at longer wavelengths dominates the spectrum. In order to isolate SHG, the spectrum has been decomposed into SH and

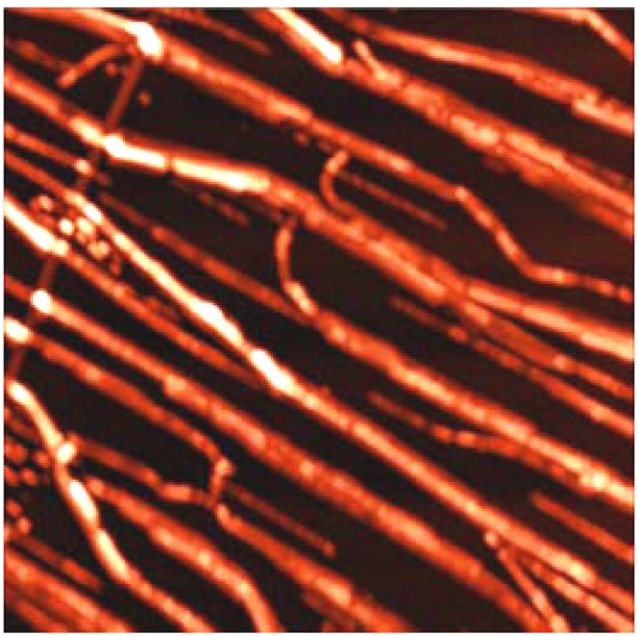

Fig. 2 $22 \times 22\ \mu m^2$ scan of a MOCNP4 sample. The average width and height of the fibers is 400 and 120 nm, respectively

Table 1 Coverage and $\sqrt{\langle h^2 \rangle}$ determined from AFM scans of the nanofiber films together with the effective nonlinear susceptibilities

	MOCNP4	CNHP4	MOCLP4
Coverage (%)	47	21	20
$\sqrt{\langle h^2 \rangle}$ (nm)	122 ± 21	593 ± 80	119 ± 18
$\chi^{(2)}_{\text{eff}}$ $(\frac{\text{pm}}{\text{V}})$	0.9 ± 0.5	1.6 ± 0.8	0.6 ± 0.3

two-photon PL contributions represented by Gaussians. The PL part of the spectrum consists of a series of vibrational modes that decay in intensity as the energy moves below the band gap. In the present case five modes have been used to represent the spectrum.

The nanofibers grow along a preferred direction of the mica substrate as shown by AFM. This is also seen in the nonlinear optical signals as a dependence on the polarization direction of the pump light. Figure 4 shows the variation of both the SHG and the PL signals as functions of the polarization direction of the 720-nm pump field. The signals follow $\cos^4(\phi)$ dependencies where ϕ is the angle between the preferred direction of the molecules and the direction of the field. The relatively small signal at $\phi = 90°$ indicates a high degree of order in the arrangement of the fibers on the substrate. Furthermore, the rotational dependence indicates that only one component of the nonlinear response, namely the polarizability along the long axis of the molecules, usually designated $\chi^{(2)}_{zzz}$, needs to be considered.

In addition to anisotropy from the molecular structure of the fibers the contrast in dielectric constant of the fiber material and the surroundings media is expected to lead to anisotropy in SHG recorded with the pump field parallel and perpendicular to the fibers. Such an effect was observed by Wang et al. [9] for indium phosphide nanowires and investigated both theoretically and experimentally by Shik et al. [10–13]. The component of the applied field parallel to the fiber is the same inside and outside the fiber while the perpendicular component will be reduced by the factor

$$a(n_\mathrm{m}) = 2n_\mathrm{m}^2/\left(n_\mathrm{m}^2 + n_\mathrm{f}^2\right), \tag{1}$$

where n_m and n_f are the refractive indices of the surrounding medium and the fiber, respectively. This expression is derived for cylindrical wires with diameters much smaller than the wavelength of light. In the present case this may not be a good approximation since the fibers have the shape of a discontinuous film rather than a cylindrical wire and the width of the fibers is comparable to the wavelength (see Fig. 2). In order to estimate effects of the dielectric mismatch the rotational anisotropy was measured with glycerol (refractive index $n_\mathrm{gl} = 1.47$) as index matching placed between the sample surface and a glass plate. The glass plate alone did not change the anisotropy. However, with the glycerol layer the anisotropy, measured as the ratio between maximum and minimum signals, increased by a factor 1.6 for CNHP4, 1.2 for MOCNP4, while the effect of index matching was negligible for MOCLP4.

The description above does not take the effects of the fiber geometry discussed earlier into account. When (1) is plotted a linear dependence on n_m that to a reasonable approximation follows $a(n_\mathrm{m}) = a(1) + \alpha(n_\mathrm{m} - 1)$ is obtained. In order to correct our calculations of $\chi^{(2)}_\mathrm{eff}$ for the field factor we need to determine $a(1)$. Assuming $a(n_\mathrm{f}) = 1$ and using the ratio $a(n_\mathrm{gl})/a(1)$ determined from the index matching experiments it is possible to estimate $a(1)$ for each of the fibers: $a(1) = 0.78$ for CNHP4 and $a(1) = 0.89$ for MOCNP4. Here the refractive index $n_\mathrm{f} = 2.2$ of *para*-hexaphenylene films [18] has been used. Thus, the pump field inside the fibers is reduced by the factor $a(1)$ when the experiments are performed without index matching as it is the case in the following. The spectroscopy has been performed with the pump field being polarized perpendicular to the fibers since this gives the strongest nonlinear signals. Effects of dielectric mismatch must thus be taken into account in the evaluation of the data.

In order to distinguish between SHG and various luminescence processes a set of scans have been recorded where the monochromator has been tuned over a broad region containing the SH wavelength for a series of pump wavelengths

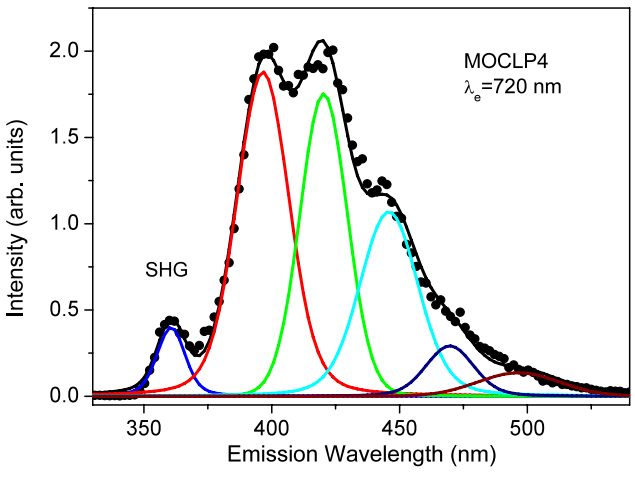

Fig. 3 Emission spectrum of MOCLP4 excited with 720-nm light. The peak at 360 nm is SHG while the remaining peaks are caused by phonon modes. The fully drawn curves are fits of Gaussians to the data

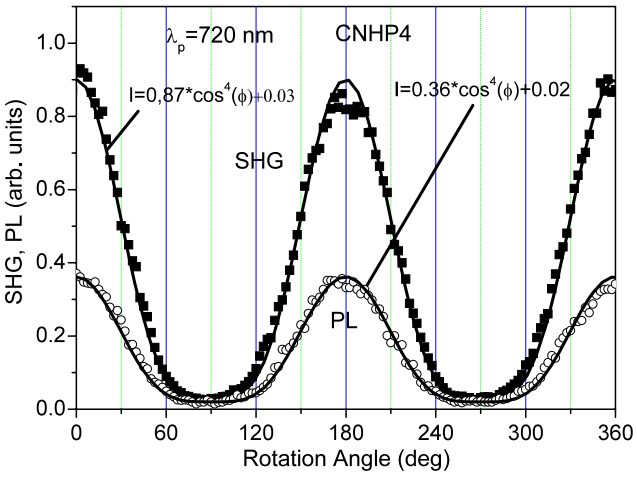

Fig. 4 Rotational scans of the polarization direction of the pump light relative to the preferred direction of the CNHP4 sample. The signals have been recorded at 360 nm for SHG and 430 nm for PL

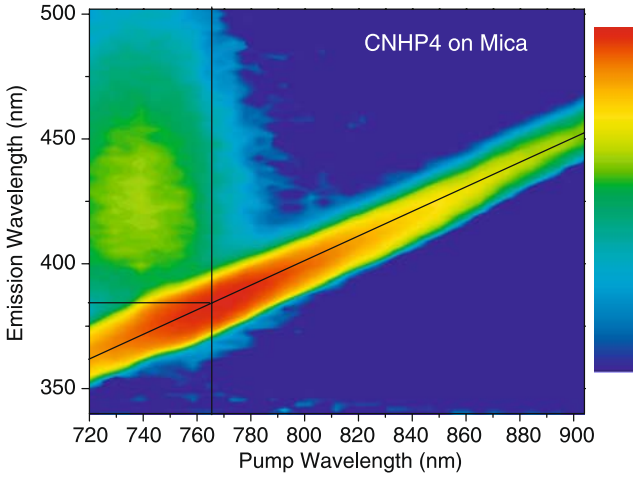

Fig. 5 Contour plot showing on a logarithmic scale the up-converted light emission intensity as a function of the pump wavelength for the CNHP4 sample. The signal is normalized to a quartz reference and shown on a logarithmic scale. Structures due to SHG and two-photon PL are seen. The peak in SH intensity is marked by a *vertical line*. The color codes cover the range from 0.05 (*blue*) to 33 (*red*)

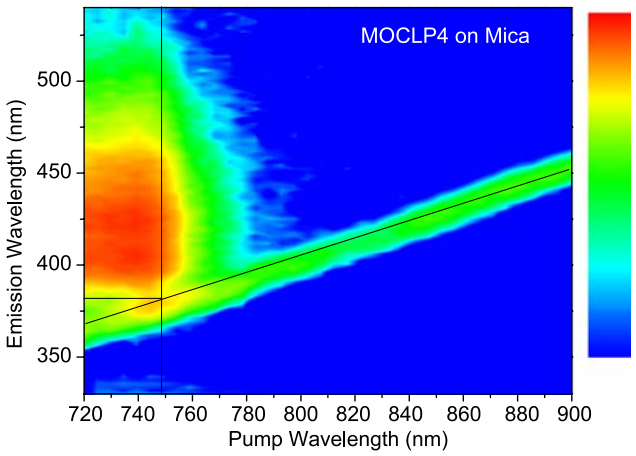

Fig. 6 Contour plot showing on a logarithmic scale the up-converted light emission intensity as a function of the pump wavelength for the MOCLP4 sample. The signal is normalized to a quartz reference and shown on a logarithmic scale. Structures due to SHG and two-photon PL are seen. The peak in SH intensity is marked by a *vertical line*. The color codes cover the range from 0.005 (*blue*) to 1.8 (*red*)

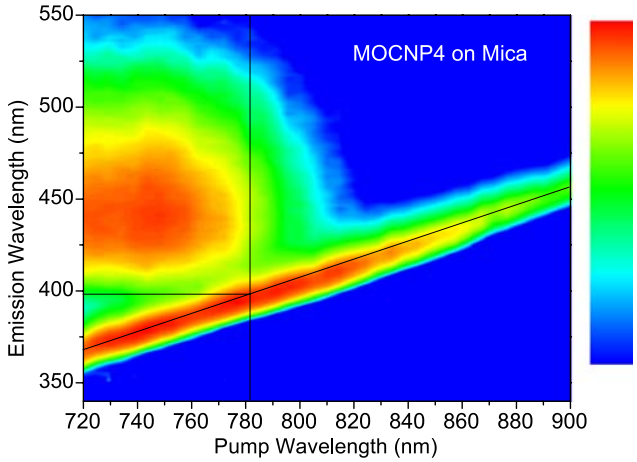

Fig. 7 Contour plot showing on a logarithmic scale the up-converted light emission intensity as a function of the pump wavelength for the MOCNP4 sample. The signal is normalized to a quartz reference and shown on a logarithmic scale. Structures due to SHG and two-photon PL are seen. The peak in SH intensity is marked by a *vertical line*. The color codes cover the range from 0.01 (*blue*) to 0.8 (*red*)

between 720 and 900 nm with 5-nm intervals. Figures 5, 6, 7 show contour plots generated from these data. Before the contour plots were generated the individual scans were normalized to the SHG signal from a quartz reference. In order to enhance the different structures in the spectra the signals are shown on logarithmic scales. The plots show the differences in relative SHG and PL contributions to the signal and the wavelength of maximum PL. While SHG dominates for CNHP4 (diagonal line in the plot) it is the PL signal that contributes strongest to the MOCLP4 spectra.

Using a separation of the spectra in Figs. 5–7 into SHG and PL contributions as illustrated in Fig. 3 the SH signal as a function of SH photon energy can be deduced. Figure 8 shows the SHG spectra of the three fibers along with fits of Lorentzians to the data. The signals are specified relative to the reflected signal from a wedge shaped quartz crystal. The peaks of the nonlinear response appear at SH wavelengths of 391 nm (3.17 eV) for MOCNP4, 386 nm (3.21 eV) for CNHP4, and 374 nm (3.32 eV) for MOCLP4. Figures 5–7 demonstrate the usual shift between absorption and emission spectra. In the figures the pump wavelengths corresponding to SH peaks are marked by vertical lines. It is expected that peaks in the nonlinear response appear when the SH photon energy coincides with the lowest two-photon absorption transition. Additional peaks may appear at higher energies corresponding to higher vibrational levels in the upper state. This might explain the structure at higher energy for the MOCNP4 sample. When we consider the PL part of the figures this drops very fast when the two-photon excitation energy falls below the absorption threshold. The horizontal lines in the figures represent the same thresholds on the emission scales and thus the lower wavelength limits for the PL process.

It should be noted that the separation into SHG and PL signals has to be based on spectroscopy using a broad range of pump wavelengths. Figure 3 shows the case where the signal at the SHG peak (360 nm) appears with little PL background. It is thus fairly easy to decompose the signal into the contributions shown on the figure. However, at longer pump wavelengths (e.g., 750 nm) the decomposition is not as obvious as it can be seen from Fig. 6. One can then use the spectral components found at 720 nm to guide the decompo-

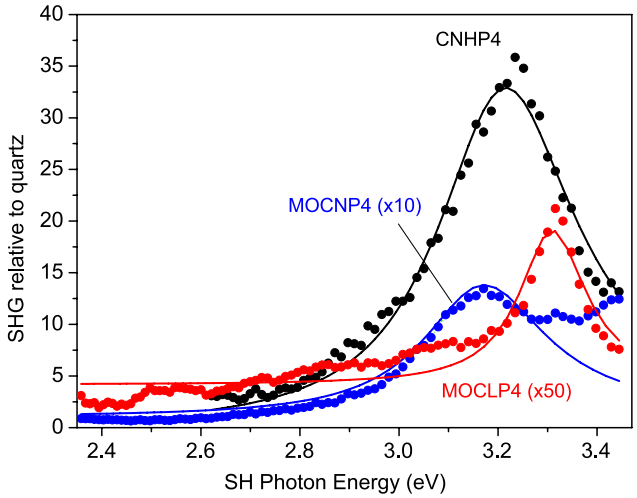

Fig. 8 Transmitted SHG from the nanofiber samples as a function of the SH photon energy. The signals are normalized to the reflected SH signal from a wedge-shaped quartz crystal. Notice the different scaling factors of the three curves. The *solid curves* are fits of Lorentzians that help to determine resonance positions

sition in the case of stronger overlap of SHG and two-photon PL.

In order to quantify the data and to compare magnitudes of the nonlinear responses the structures of the films have to be taken into account. Furthermore, in order to estimate absolute values of the nonlinear susceptibilities models for the SH signals in transmission through the nanofiber samples and in reflection from the quartz wedge have to be analyzed. SHG in transmission from thin nonlinear films has been described by several authors over the years [19–22]. These models contain transmission of pump light into the nonlinear film and the transmission of the SH light out of the film through the substrate. In the nonlinear material a 'forced' and a 'free' contribution to the SH field propagating with different phase velocities are generated. This leads to alternating constructive and destructive interference as a function of depth into the material [19]. However, for small film thicknesses compared to the wavelength of the light the two contributions will add in phase and the SH field will grow linearly with the film thickness. As demonstrated by Brewer et al. [16] the nanofibers used here fall in this regime. By using the work by Herman and Hayden [22] on SHG in transmission from a slab to describe SHG from the fibers and Bloembergen and Pershan's work [19] for the quartz wedge the ratio between nanofiber and quartz signals is given by

$$\frac{T_{\text{fiber}}}{R_{\text{quartz}}} = \frac{(I_{2\omega}/I_{\omega}^2)_{\text{fiber}}}{(I_{2\omega}/I_{\omega}^2)_{\text{quartz}}} = t_{\text{af}}^4 T_{\text{fs}}^2 T_{\text{sa}}^2 a^4 \left(\frac{2\pi L}{\lambda}\right)^2 \times \frac{(N_{\text{q}}+1)^2(n_{\text{q}}+N_{\text{q}})^2}{N_{\text{f}}^2} \left(\frac{\chi_{\text{eff}}^{(2)}}{\chi_{\text{q}}^{(2)}}\right)^2, \quad (2)$$

where n and N are the refractive indices at the fundamental and SH wavelengths, respectively and index f and q refer to the fiber material and quartz, respectively. The corresponding nonlinear susceptibilities are denoted $\chi_{\text{eff}}^{(2)}$ for the fiber material and $\chi_{\text{q}}^{(2)}$ for quartz. Transmission coefficients at the fundamental and SH wavelengths are denoted as t and T, respectively, and subscripts af, fs, and sa refer to air-film, film-substrate, and substrate-air interfaces, respectively. The field factor a determined from index matching of the rotational anisotropy has been introduced in order to take the reduction of the pump field due to the fiber geometry into account.

Absolute values of the SH reflection coefficient can be calculated using the value $\chi_{xxx}^{(2)} = 0.62$ pm/V reported for quartz by Hagimoto and Mito [21] for an excitation wavelength of 633 nm. Without precise knowledge about the refractive index of the fibers the value $n_1 = 2.2$ and $N_1 = 2.7$ corresponding to *para*-hexaphenylene films [18] have been used. Using the measured signals relative to quartz in Fig. 8 together with the coverages and the average of the square thicknesses from (Table 1) the peak values of $\chi_{\text{eff}}^{(2)}$ for the three different fiber materials shown in Table 1 have been estimated. These values include the estimated field factors. In the analysis absorption in both the nanofiber film and the mica substrate has been neglected. However, comparison of experiments performed with the nanofibers on the input and output side of the mica substrate only show a small difference in SH intensity consistent with reflection losses for the pump beam when the nanofibers are on the output side. This is further supported by transmission measurements on the samples. The uncertainty in estimating the nonlinear susceptibilities in Table 1 results from the spread in the height of the nanofibers measured at different places on the sample together with the rough estimate of effects of the fiber geometry on the fundamental fields in the fibers. This uncertainty is considerably larger than that of the relative measurements between sample and quartz reference.

Nonlinear optical spectroscopy has previously been reported on the three types of nanofiber films considered here in Ref. [16, 17]. Though the spectroscopy by Brewer et al. [16] was based on a limited number of wavelengths there is agreement with the present work concerning the general trends in the relative positions of the peaks in the nonlinear response. With respect to absolute magnitudes of the nonlinear susceptibilities compared to those reported by Brewer et al. [16] the results for MOCNP4 and MOCLP4 are a factor of two higher in the present work. However, considering that the samples are not the same and the uncertainty introduced by the procedure that takes the film structure into account the two sets of experiments are in reasonable agreement.

Two of the functionalized molecular building blocks (CNHP4 and MOCNP4) contain a cyano electron pull group

in one end. Furthermore, the MOCNP4 molecule has an electron push methoxy group at the other end. One might expect that the MOCNP4 molecule with both an electron pull and electron push group would have the highest dipole moment and thus the highest nonlinearity. This seems, however, not to be transferred to $\chi^{(2)}_{\text{eff}}$ of the material. The reason could be differences in the structure of the materials either on the molecular level or in the orientational order of the fibers. By comparing the data for MOCNP4 and MOCLP4 it can be seen that the cyano end group leads to a stronger nonlinearity than the chlorine end atom. This is also expected since the cyano group is highly electronegative and thus very efficient in generating molecular dipoles. Furthermore, with the Cl end atom the resonance shifts to higher energies. This is also expected since Cl contrary to the cyano group does not contribute to the conjugated chain and thus effectively leads to a shorter molecule. A simple confinement consideration predicts a higher resonance frequency for shorter molecules.

4 Conclusions

Detailed mappings of nonlinear emission spectra from functionalized *para*-phenylenes as a function of the excitation wavelength have been carried out. The contributions to SHG have been isolated on a strong background of two-photon photoluminescence. Furthermore, it has been shown that some effects of the fiber geometry on the field inside the nanofibers are present and the effect on the nonlinear response can be estimated from index matching experiments. The SH spectra show well-defined resonances in the range from 3.17 to 3.32 eV depending on the end groups of the molecules.

For all three materials SHG appears together with strong two-photon luminescence (see Figs. 5–7). By pumping the fibers below the onset of the two-photon process complete dominance of the SHG process is obtained. However, resonant enhancement of SHG is inevitably accompanied by luminescence. Nevertheless, our experiments demonstrate that considerable enhancement of SHG over luminescence is obtained by proper choice of functionalization, e.g., CNHP4. For this material the nonlinear susceptibility is comparable to that found for inorganic nonlinear optical crystals.

Acknowledgements We thank I. Wallmann, University of Bonn, for providing CNHP4, and M.S. thanks A. Lützen, University of Bonn, for excellent working conditions for the synthesis of MOCNP4 and MOCLP4. J. Brewer, University of Southern Denmark, and Thomas Garm Pedersen, Aalborg University, are thanked for helpful discussion on data evaluation and on the manuscript. Two of us, M.S. and H.G.R., thank the Danish Research Agency under FTP and FNU grants as well as the Danish National Advanced Technology Foundation, HTF, for supporting this work.

References

1. M. Schiek, F. Balzer, K. Al-Shamery, J.R. Brewer, A. Lützen, H.-G. Rubahn, Small **4**, 176 (2008)
2. M. Schiek, K. Al-Shamery, A. Lützen, Synthesis of symmetrically an unsymmetrically para-functionalized p-quaterphenylenes, Synthesis, 613–621 (2007)
3. I. Wallmann, M. Schiek, R. Koch, A. Lützen, Synthesis, 2446–2450 (2008)
4. J. Brewer, M. Schiek, A. Lützen, K. Al-Shamery, H.-G. Rubahn, Nano Lett. **6**, 2656 (2006)
5. M. Schiek, F. Balzer, K. Al-Shamery, A. Lützen, H.-G. Rubahn, Soft Matter. **4**, 277–285 (2008)
6. K. Pedersen, S.I. Bozhevolnyi, J. Arentoft, M. Kristensen, C. Laurent-Lund, J. Appl. Phys. **88**, 3872 (2000)
7. J.A. Long, B.S. Simpkins, D.J. Rowenhorst, P.E. Pehrsson, Nano Lett. **7**, 831 (2007)
8. S.W. Chan, R. Barille, J.M. Nunzi, K.H. Tam, Y.H. Leung, W.K. Chan, A.B. Djurisic, Appl. Phys. B **84**, 351 (2006)
9. J. Wang, M.S. Gudiksen, X. Duan, Y. Cui, C.M. Lieber, Science **293**, 1455 (2001)
10. H.E. Ruda, A. Shik, Phys. Rev. B **72**, 115308 (2005)
11. H.E. Ruda, A. Shik, J. Appl. Phys. **100**, 024314 (2006)
12. H.E. Ruda, A. Shik, J. Appl. Phys. **101**, 034312 (2007)
13. V. Barzda, R. Cisek, T.L. Spencer, U. Philipose, H.E. Ruda, A. Shik, Appl. Phys. Lett. **92**, 113111 (2008)
14. S.I. Bozhevolnyi, J.M. Hvam, K. Pedersen, F. Laurell, H. Karlsson, T. Skettrup, M. Belmonte, Appl. Phys. Lett. **73**, 1814 (1998)
15. J. Beerman, S.I. Bozhevolnyi, V.G. Bordo, H.-G. Rubahn, Opt. Commun. **237**, 423 (2004)
16. J. Brewer, M. Schiek, I. Wallmann, H.-G. Rubahn, Opt. Commun. **281**, 3892 (2008)
17. J. Brewer, Development and nanophysical applications of ultrashort-pulse higher harmonic optical microscopy. Ph.D. thesis, University of Southern Denmark, 2007
18. C. Suess, F.P. Wenzl, G. Jakopic, M. Muehlegger, N. Koch, A. Haase, K. Lamprecht, M. Schatzmayr, C. Mitterbauer, F. Hofer, G. Leising, Surf. Sci. **507–510**, 473 (2002)
19. N. Bloembergen, P.S. Pershan, Phys. Rev. **128**, 606 (1962)
20. J. Jerphagon, K. Kurtz, J. Appl. Phys. **41**, 1667 (1970)
21. K. Hagimoto, A. Mito, Appl. Opt. **34**, 8276 (1995)
22. W.N. Herman, L.M. Hayden, J. Opt. Soc. Am. B **12**, 416 (1995)